# I&EC research

**Industrial & Engineering Chemistry Research**

Article

# Experimental Evaluation of a Chinese Sulfur-Containing Lean Iron Ore as the Oxygen Carrier for Chemical-Looping Combustion

Xiaojia Wang,[†,‡] Hao Liu,*[,‡] Baosheng Jin,*[,†] Jie Zhao,[†] Chenggong Sun,[‡] and Colin E. Snape[‡]

[†]Key Laboratory of Energy Thermal Conversion and Control of Ministry of Education, School of Energy & Environment, Southeast University, Nanjing 210096, People's Republic of China

[‡]Faculty of Engineering, University of Nottingham, Nottingham NG7 2RD, U.K.

**Ⓢ** *Supporting Information*

**ABSTRACT:** A series of chemical-looping combustion (CLC) tests were conducted in a thermogravimetric analysis (TGA) reactor to investigate the potential of a Chinese sulfur-containing lean iron ore as the oxygen carrier. Two main products of solid-fuel pyrolysis and gasification, namely, $CH_4$ and $CO$, were selected as the reducing gases. Consecutive reduction—oxidation cycles were first carried out in the TGA reactor to evaluate the cyclic stability and agglomeration tendency of the oxygen carrier. The effects of the temperature, fuel gas concentration, and reaction gas composition on the reduction reaction were further investigated. Increasing the reaction temperature or fuel gas concentration enhanced the reduction rate and reaction degree of the oxygen carrier. Meanwhile, $CO$ showed much higher reduction reactivity than $CH_4$. A comparison of the rate index of the iron ore used with those of high-grade minerals indicated that the iron ore had adequate reactivity for its application in solid-fuel CLC technology. The side reaction of carbon deposition was also discussed. Finally, the shrinking-core model with chemical reaction control was adopted to determine the chemical kinetics.

## 1. INTRODUCTION

Owing to its inherent feature of separating $CO_2$ without extra energy loss during the combustion process, chemical-looping combustion (CLC) has been regarded as a promising novel combustion technology for $CO_2$ capture.[1,2] At present, there is an increasing interest for solid-fuel CLC because of the lower price and more abundant reserves of solid fuels (e.g., coal and biomass) compared with gaseous fuels.[3−7] One of the promising configurations of solid-fuel CLC is to introduce solid fuels into the fuel reactor directly so that gasification of the solid fuel and subsequent reduction of the oxygen carrier (OC) are integrated in the fuel reactor.[8−13]

The selection of an appropriate OC plays an important role in the successful operation of a CLC system. Previous studies have mainly focused on the synthetic (man-made) OCs with some metal oxides (e.g., CuO, NiO, CoO, $Fe_2O_3$, or $Mn_3O_4$) as the primary active components.[14−18] These OCs are usually supported on different inert materials such as $Al_2O_3$, $SiO_2$, $TiO_2$, and $ZrO_2$ to enhance their reactivity.[19] Most of the synthetic OCs perform well with favorable reactivity, high mechanical strength, and low tendency for agglomeration in CLC systems with gaseous fuels. Meanwhile, these synthetic OCs also exhibit a wide range of oxygen-transport capacities varying with the content of inert materials in the OCs (e.g., 0.02 for Cu10Al-I[16] due to the inclusion of 90 wt % $Al_2O_3$ compared to 0.2 for pure CuO).[14−19] So far, several research teams have successfully demonstrated the feasibility of synthetic OCs in different gas-fuel CLC pilot-scale reactors.[20−23]

OC loss is an important factor that needs to be considered when selecting OCs for CLC systems, and, in fact, it can determine the viability of an OC for a specific CLC system. In a gas-fuel CLC system, the loss of an OC mainly comes from attrition during the fluidization and circulation processes.[20−23]

However, in a solid-fuel CLC system, the regular drain of fuel ash from the system to avoid its accumulation will inevitably result in an extra loss of OC particles.[24] Moreover, deactivation of the OC may also happen because of the presence of organic sulfur in solid fuels.[11−13] Therefore, compared with gas-fuel CLC technology, solid-fuel CLC technology will face a more serious issue in much larger mass loss of the OC. For future large-scale solid-fuel CLC applications, the cost of the OC may become the decisive factor in the selection of the OC considering the huge quantity of OC needed and the large amount of OC loss during operation. In this context, some low-cost iron-based natural minerals (e.g., ilmenite, hematite, and iron ore) have been attracting more and more attention for their applications in solid-fuel CLC technology. Leion et al.[5] found that the ilmenite supplied by Titania A/S (Norway) showed high reactivity with solid fuels in a fluidized-bed reactor. Berguerand and Lyngfelt[4,25−27] investigated the performance of ilmenite in a 10 $kW_{th}$ CLC combustor with different fuels, temperatures, and particle circulations. They concluded that ilmenite should be a suitable OC material for the solid-fuel CLC system. Monazam et al.[28] performed thermogravimetric analysis (TGA) of the reduction behavior of hematite with one of the main gases from coal gasification (i.e., CO) under conditions of different concentrations and temperatures. Xiao et al.[7] investigated the reaction performance of Companhia Vale Do Rio Doce iron ore (from Brazil) under pressurized conditions in a laboratory fixed-bed reactor. They found that the pressure played a positive role in increasing the
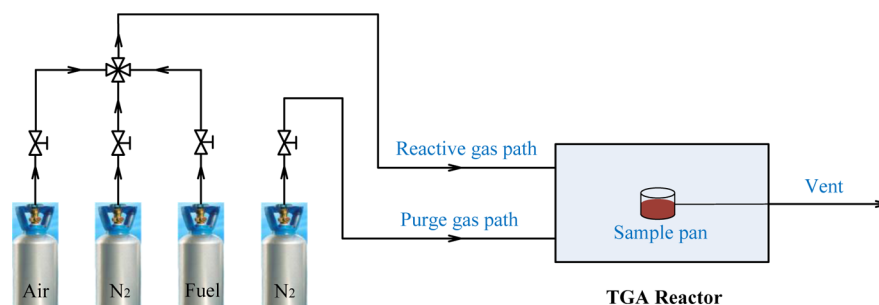
**Figure 1.** Schematic layout of the laboratory TGA reactor system.

$CO_2$ concentration and promoting OC conversion. They also built a pilot-scale pressurized solid-fuel CLC unit and conducted continuous tests using Mining Area C iron ore (from Australia) as the OC, which proved the feasibility of coal-fueled pressurized CLC with iron ore as the OC.[29]

The results of the previous investigations have indicated that iron-based natural minerals are promising OCs for future large-scale solid-fuel CLC applications. However, it should be noted that most of these natural iron-based OCs are high-grade iron-based minerals with high iron contents. In many places around the world, especially in China, there is much more abundant storage of lean iron ores than of high-grade iron minerals. The lean iron ores have more advantage in price, but as the name implies, they contain lower iron and more impurities such as inerts and sulfur, which may make them unsuitable as OCs or make the CLC reactions much more complex when they are used as OCs. Hence, there is a need to carry out feasibility studies of CLC using lean iron ores as the OCs.

In this work, a Chinese lean iron ore with low iron content but high $CaSO_4$ content was selected as the OC. The main aim of this study is to investigate the CLC performance of this iron ore with two main gases from the pyrolysis and gasification of solid fuels (i.e., $CH_4$ and CO). Consecutive reduction−oxidation cycles were first performed in a TGA reactor to evaluate the cyclic stability and agglomeration tendency of the OC. The effects of the reaction temperature, fuel gas concentration, and fuel gas composition on the reduction reaction were further thoroughly investigated. Then the reactivity of the lean iron ore was evaluated by comparing its rate index with those of the high-grade hematite and ilmenite. The side reaction of carbon deposition was also discussed. Finally, a comprehensive kinetics model was developed to determine the kinetics of the reduction reaction for the investigated iron ore OC.

## 2. EXPERIMENTAL SECTION

**2.1. Materials.** The OC selected is a natural iron ore from Harbin, Heilongjiang Province, China. Prior to the experiments, the iron ore was crushed and sieved to a broad size range of 0.25−0.65 mm and then calcined at 970 °C for 2 h under an oxidizing atmosphere. The calcination treatment can help to improve the properties and reactivity of the OC and avoid defluidization problems.[4,24,30,31]

According to the X-ray fluorescence (XRF) spectrometry characterization (Table S1), the main reactive components of the calcined iron ore are $Fe_2O_3$ (35.21%) and $CaSO_4$ (10.00%). The other main components include inert $SiO_2$ (38.26%), $Al_2O_3$ (8.22%), and some other materials. The characterization

result from XRF is consistent with that of X-ray diffraction analysis. The apparent density of the calcined iron ore is 2558 kg/m$^3$, and the bulk density is 1535 kg/m$^3$.

**2.2. TGA Experimental Setup and Procedure.** As shown in Figure 1, the experiments were carried out in a thermogravimetric analyzer (SDT Q600). $CH_4$ and CO diluted in nitrogen ($N_2$) to different concentrations were used as the gaseous fuels (i.e., 20% $CH_4$, 50% $CH_4$, 100% $CH_4$, 10% CO, and 20% CO). Air and high-purity $N_2$ (99.99%) were used as the oxidizing and purge gases, respectively. Table S2 details the gases used in the experiments.

Prior to each test, the OC sample (about 60 mg) was placed on a quartz pan centered in the gas inlet and exit ports of the reaction tube. At the beginning of the test, the sample was heated at a heating rate of 20 °C/min to the desired reaction temperature and held for 20 min under the $N_2$ environment. Then the fuel gas and air were alternately introduced into the reaction tube with the high-purity $N_2$ as the purge gas in between to prevent the reducing gas ($CH_4$ or CO) and the oxidizing agent (air) from mixing. During the whole testing process, the weight variation of the samples and the reaction temperature were measured and recorded in real time with the TGA reactor system.

**2.3. Data Evaluation.** *2.3.1. Conversion of the OC and Oxygen-Transport Capacity.* Conversion of the OC for the reduction reaction ($X$) is the ratio of the actual mass loss to the usable oxygen mass in the OC:

$$X = \frac{m_{ox} - m}{m_{ox} - m_{red}} = \frac{m_{ox} - m}{R_O m_{ox}} \tag{1}$$

where $m$ is the instantaneous mass of the OC, $m_{ox}$ is the mass of OC in the completely oxidized state, and $m_{red}$ is the mass of OC in the completely reduced state. $R_O$ is the oxygen-transport capacity, representing the mass fraction of usable oxygen in the OC during the oxygen-transfer process.

$$R_O = \frac{m_{ox} - m_{red}}{m_{ox}} \tag{2}$$

$$R_O = R_{Fe_2O_3} x_{Fe_2O_3} + R_{CaSO_4} x_{CaSO_4} \tag{3}$$

where $R_{Fe_2O_3}$ is the oxygen-transport capacity of $Fe_2O_3$ when converted to iron ($R_{Fe_2O_3}$ = 30%) and $R_{CaSO_4}$ is the oxygen-transport capacity of $CaSO_4$ when converted to CaS ($R_{CaSO_4}$ = 47.06%). $x_{Fe_2O_3}$ and $x_{CaSO_4}$ are the mass fractions of $Fe_2O_3$ and $CaSO_4$ in the OC, respectively. Hence, the oxygen-transport capacity for the OC used $R_O$ can be calculated to be 15.27%.

*2.3.2. Applicable Conversion of the OC and Oxygen-Transport Capacity.* In CLC applications, because of the thermodynamic limitation, complete conversions of CO and $H_2$ toward $CO_2$ and $H_2O$ can be achieved only when free $Fe_2O_3$ is just reduced to the state of $Fe_3O_4$.[16,19,24] Thus, the applicable oxygen-transport capacity for the investigated iron ore, i.e., $R_{O,ap}$, is defined considering that in the reduced state iron is present as $Fe_3O_4$.[24]

$$R_{O,ap} = \frac{m_{ox} - m_{red,ap}}{m_{ox}} \qquad (4)$$

where $m_{red,ap}$ is defined as the mass of the OC in the specific reduced state when $Fe_2O_3$ contained in the OC is completely transformed to $Fe_3O_4$. However, because of the synchronous existence of the reduction reaction of $CaSO_4$, it is impossible to identify this point exactly with the TGA method. In this study, we assume that the specific reduced state is reached when the measured mass loss of the OC equals the transferred mass of oxygen from $Fe_2O_3$ to $Fe_3O_4$. Thus, the value of $R_{O,ap}$ can be calculated to be 1.174%.

The applicable conversion of the OC for the reduction reaction $(X_{ap})$ refers to the ratio of the mass loss of the OC to a part of the specific oxygen mass in the OC that is applicable for the industrial CLC applications:[24]

$$X_{ap} = \frac{m_{ox} - m}{m_{ox} - m_{red,ap}} = \frac{m_{ox} - m}{R_{O,ap} m_{ox}} \qquad (5)$$

*2.3.3. Rate Index.* The rate index $\phi$ is usually adopted to evaluate the reactivity of the OC.[24]

$$\phi = 100 \times 60 \times R_{O,ap} \left( \frac{dX_{ap}}{dt} \right) \qquad (6)$$

## 3. RESULTS AND DISCUSSION

**3.1. Reactivity of the OC.** *3.1.1. Cyclic Stability.* The cyclic stability of an OC refers to its lasting reaction performance throughout continuous redox cycles. Hence, it is an important consideration for selection of the OCs in CLC systems. The cyclic stability of the lean iron ore has been evaluated by successive cycles of reduction and oxidation in the TGA reactor.

Figure 2 gives an example of the successive redox cycles of the lean iron ore under a specific set of conditions, with the reduction reaction performed at 950 °C in 10% CO and the
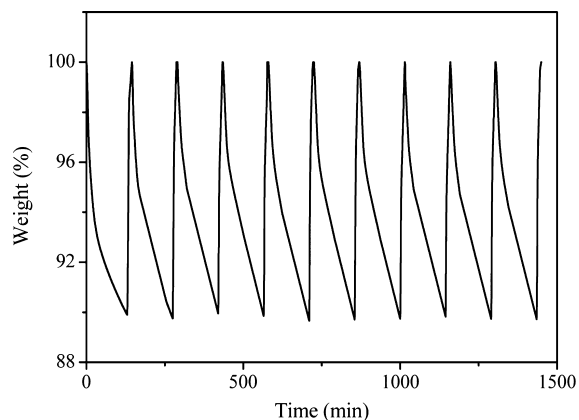
**Figure 2.** TGA of the calcined iron ore in successive redox cycles.

oxidation reaction at 950 °C in air. It can be observed that the rate of the oxidation reaction is obviously higher than that of the reduction reaction. At the same time, the reduction and reoxidation curves in the successive cycles are repeatable with very similar oxygen-transport capacities. Such consistency indicates the stable performance of the iron ore throughout the continuous redox cycles. A similar cyclic stability of the investigated iron ore has also been observed under other conditions with different reaction gas compositions, concentrations, and temperatures. Moreover, no obvious weight loss of OC was detected through the successive redox cycles, indicating that the release of $SO_2$ should be restrained and, hence, the oxygen-transport capacity of the OC was maintained. This is probably attributed to the high contents of $Fe_2O_3$[32] and inert supports (e.g., $SiO_2$)[33] in the OC as well as the suitable reaction temperatures (i.e., ≤950 °C),[32−34] which can effectively decrease the risk of sulfur release. Similar findings have also been reported in the previous literature.[33,34]

On the other hand, we can further observe small increases in the reaction degree as the number of cycles increases. The reactivity increase of the OC with consecutives redox cycles can be explained through the change of the crystal structure of the OC. Figure 3 shows scanning electron microscopy (SEM) photographs of the calcined iron ore samples before and after redox cycles. It can be found that granulation is enhanced after consecutives cycles, which leads to a higher surface area for the reaction and, hence, an increase in the reactivity of the OC. In addition, there is an increase in the porosity of the OC through the appearance of macropores or cracks with the redox cycles, which is also important for the reactivity increase. The above observations are in agreement with the previous investigations.[24,35,36]

Finally, the calcined iron ore samples did not show any agglomeration during the continuous reduction/oxidation cycles.

*3.1.2. Effect of the Temperature.* The temperature is the most important operating parameter in the reactions of CLC. Hence, the effect of the temperature on the reduction reaction of the OC was carried out under different reaction temperatures of 800, 850, 900, and 950 °C. In this section, 50% $CH_4$ was selected as a representative of fuel gases for analysis.

Figure 4 shows conversion of the iron ore used during the reduction process as a function of time under different temperatures. It can be observed that conversion of the OC at 60 min is only 25.08% at 800 °C. However, when the temperature increases to 950 °C, conversion can reach 94.44%, indicating that reduction of the OC is close to the completely reduced status. Clearly, the reaction temperature has a strong effect on the reduction reaction. The increase in the temperature enhances the reaction rate and promotes the degree of reduction. Moreover, the effect becomes more significant at higher temperatures. The variations of the OC conversion under different temperatures are in agreement with those of other investigations.[28]

According to the above observations, the suitable temperature for higher reduction reactivity in the fuel reactor seems to be around 950 °C. However, it should be noted that, for the cases of 50% $CH_4$ and 100% $CH_4$, carbon deposition was observed at the end of the reduction reaction when the operating temperature was at 950 °C. For future solid-fuel CLC systems, only the transformation from $Fe_2O_3$ to $Fe_3O_4$ is desirable in order to get full fuel gas conversion and the concentration of $CH_4$ is unlikely to exceed 20%; therefore, the
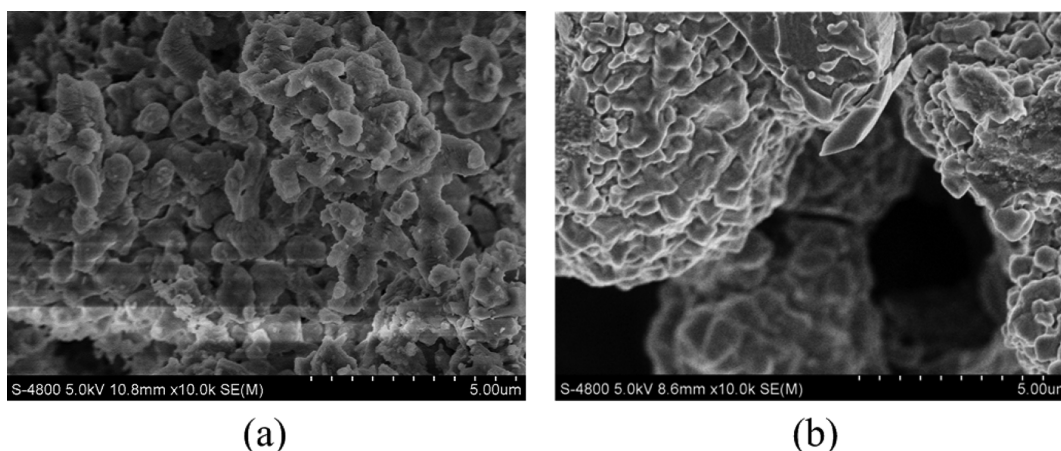
**Figure 3.** SEM images of calcined iron ore: (a) before reaction; (b) after five redox cycles.
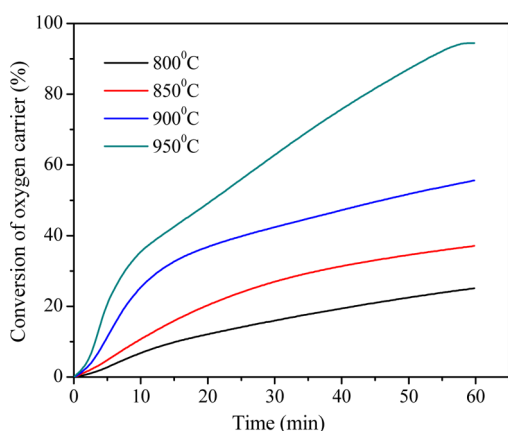


**Figure 4.** Effect of the reaction temperature on conversion of the OC as a function of time. $CH_4$ concentration = 50%.

appearance of carbon deposition becomes almost impossible in practice.[16,19,37−39] This point will be addressed in more detail later in section 3.2.

*3.1.3. Effect of the Reaction Gas Concentration.* In this section, three cases (20%, 50%, and 100% $CH_4$ under 850 °C) were selected as representatives to investigate the effect of the reaction gas concentration on the reduction reaction. Figure 5 exhibits the variations of the OC conversion with time under
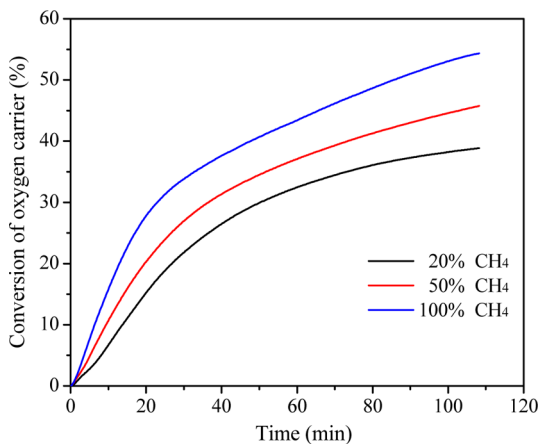


**Figure 5.** Effect of the reaction gas concentration on the conversion of the OC as a function of time. $T$ = 850 °C.

different $CH_4$ concentrations. First, increasing the concentration of $CH_4$ leads to an increase in the reduction reaction rate and an increase in the reaction degree of the iron ore. The OC conversion is 38.87% for 20% $CH_4$ and increases to 54.38% for 100% $CH_4$ at the quasi-equilibrium time of 110 min. Similar effects of fuel gas concentrations on the reaction rates and OC conversions have been observed for other reaction temperatures, although the reaction temperature can have greater impacts on the reaction rates and OC conversions, as was already shown in Figure 4.

*3.1.4. Effect of the Reaction Gas Composition.* In order to investigate the effect of the reaction gas composition on the reduction reaction, two cases with different fuel gas compositions ($CH_4$ and CO) were carried out for comparison, while the reaction temperature and fuel gas concentration were kept consistent at 850 °C and 20%, respectively. Figure 6
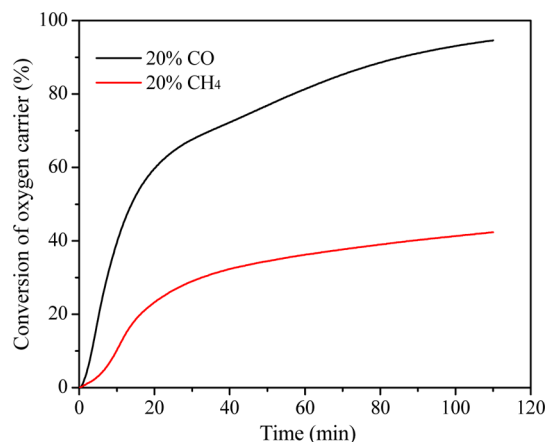


**Figure 6.** Effect of the reaction gas composition on the conversion of the OC as a function of time. $T$ = 850 °C. Gas concentration = 20%.

presents conversions of the OC during the reduction process as a function of time under different fuel gas compositions. At the quasi-equilibrium time of 110 min, the OC conversion is only 42.32% for $CH_4$, while for CO, it is 94.63%, indicating that the reduction reactivity of the iron ore on CO is much higher than that on $CH_4$.

Nowadays, the adaptation of CLC on solid fuels such as coal and biomass is becoming more and more attractive because of the much more abundant supply of solid fuels than of gaseous

fuels. However, because the slow reaction of char gasification is the rate-controlling step in solid-fuel CLC, the global reaction rate and, hence, the system thermal power will be greatly limited.[7,24] In this respect, considering that CO is the major gaseous product of char gasification, the high reactivity of the tested iron ore on CO can increase the consumption rate of CO generated from char gasification and, hence, promote the gasification rate of char and the system efficiency. Therefore, the iron ore adopted in this study can be regarded as a potential OC candidate that is more appropriate for solid-fuel CLC applications.

*3.1.5. Reactivity Comparison with High-Grade Hematite and Ilmenite.* In order to better evaluate the potential of the selected OC, we compared the reaction rate (expressed by the rate index $\phi$) of the lean iron ore adopted in this study with those of two high-grade iron minerals used in previous TGA experiments, i.e., a hematite by Monazam et al.[28] and an ilmenite by Adánez et al.[24] The main operating conditions adopted in this study for comparison (i.e., 20% CO for the fuel gas concentration and 900 °C for the reaction temperature) were consistent with those of Monazam et al.[28] Hwever, in the experiment by Adánez et al.,[24] a little lower fuel gas concentration (15% CO) was adopted.

Table 1 illustrates a comparison of the rate index among different OCs. It can be found that the rate index of the lean

**Table 1. Reactivity Comparison with Hematite[28] and Ilmenite[24]**

|  | iron content (%) | applicable oxygen-transport capacity $R_{O,ap}$ (%) | maximum value of the rate index for CO (%/min) |
|---|---|---|---|
| hematite | 57.78 | 2.75 | ~0.80 |
| ilmenite (activated) | 33.37 | 4.8 | 1.6 |
| iron ore (calcined) | 24.65 | 1.174 | 0.70 |

iron ore reaches about half that of ilmenite and is in close proximity to that of hematite. The relatively high reaction rate of the lean iron ore is mainly attributed to the rich contents of inert materials (e.g., $SiO_2$ and $Al_2O_3$), which play the role of porous supports and provide a large surface area for the gas–solid contact and reactions.[19] In addition, the reduction of $CaSO_4$ also promotes the global reaction rate of the lean iron ore. Therefore, compared with the high-grade iron minerals, the lean iron ore used in this study shows good competitiveness on the reactivity in addition to the advantage of low cost for future applications of large-scale solid-fuel CLC power plants.

**3.2. Carbon Deposition.** Carbon deposition was observed at the end of the reduction period for the cases of 50% $CH_4$ and 100% $CH_4$ at a temperature of 950 °C. The main reactions for carbon formation are shown as follows:[40−42]

$$CH_4 \rightarrow C + 2H_2 \tag{R1}$$

$$C + CO_2 \rightarrow 2CO \tag{R2}$$

$$C + H_2O \rightarrow CO + H_2 \tag{R3}$$

However, no carbon deposition was observed when the temperature was lower than 950 °C, when the concentration of $CH_4$ was lower than 50%, or when the fuel gas used was CO. Moreover, for the cases of 50% $CH_4$ and 100% $CH_4$ under a temperature of 950 °C, carbon deposition was observed only at the end of the reduction reaction process. This indicates that

carbon deposition can be restrained by using lower temperature and $CH_4$ concentration, shorter reduction time, and excess OC. These findings are in agreement with the previous literature.[42] For future solid-fuel CLC systems, only the transformation from $Fe_2O_3$ to $Fe_3O_4$ is desirable in order to get full fuel gas conversion and the concentration of $CH_4$ is unlikely to exceed 20%; therefore, the appearance of carbon deposition becomes almost impossible in practice.

**3.3. Chemical Kinetics.** According to the XRF characterization (see Table S1), the calcined lean iron ore contains two reactive compositions: $Fe_2O_3$ and $CaSO_4$. In order to achieve complete conversion of fuel gas to $CO_2$ and $H_2O$, $Fe_2O_3$ in the OC can only be reduced to $Fe_3O_4$ in the CLC applications.[16,19,37−39] Thus, it is of great importance to know the reaction kinetics of the OC during the early reduction stage in which $Fe_2O_3$ is only reduced to $Fe_3O_4$. However, because the reactions of $Fe_2O_3$ and $CaSO_4$ proceed simultaneously during the reduction process, it is almost impossible to find the exact point when $Fe_2O_3$ in the OC is just completely reduced to $Fe_3O_4$. Here we use the calculated mass loss of the OC when $Fe_2O_3$ is completely transformed to $Fe_3O_4$ without considering of the reduction of $CaSO_4$ to determine $R_{OC,ap}$. This assumption can ensure that $Fe_2O_3$ contained in the OC only be reduced to $Fe_3O_4$, no matter how rapid the reduction of $CaSO_4$ might be. Thus, the value of $R_{O,ap}$ can be calculated to be 1.174%.

In this study, the integrated rate of reduction (IRoR) method was adopted to analyze the global reduction rate of the solid reactants of the OC instead of the complex local reduction rates of $Fe_2O_3$ and $CaSO_4$.[11,43,44] Hence, the reduction reaction of the lean iron ore with $CH_4$ or CO can be summarized as the following reactions:

$$b\text{MeO} + CH_4 \rightarrow a\text{Me} + CO_2 + 2H_2O \tag{R4}$$

$$b\text{MeO} + CO \rightarrow a\text{Me} + CO_2 \tag{R5}$$
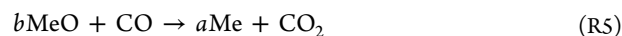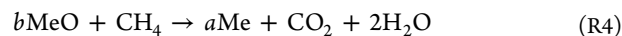
where MeO represents the solid reactants in the calcined lean iron ore (i.e., $CaSO_4$ and $Fe_2O_3$). Me represents a reduced form of MeO.

In order to determine the reaction kinetics parameters of the OC on $CH_4$ and CO, the shrinking-core model (SCM) for the spherical grain geometry of a reacting particle was adopted. The equations of the SCM under chemical reaction control in the grain are shown as follows:[16,19,45]

$$1 - (1 - X_{ap})^{1/3} = \frac{bkC^n}{\rho_m r_g} t \tag{7}$$

where $b$, $C$, $n$, $\rho_m$, and $r_g$ represent the stoichiometric coefficient, reacting gas concentration, reaction order, molar density, and grain radius, respectively. The reaction rate constant $k$ follows Arrhenius law:

$$k = k_0 \exp(-E/RT) \tag{8}$$

where $k_0$ is the preexponential factor of the rate constant, $E$ is the activation energy, and $R$ is the constant of the ideal gases, where $R$ = 8.314 J/mol·k.

The reaction rates of reaction R4 (or reaction R5) can be expressed as follows:

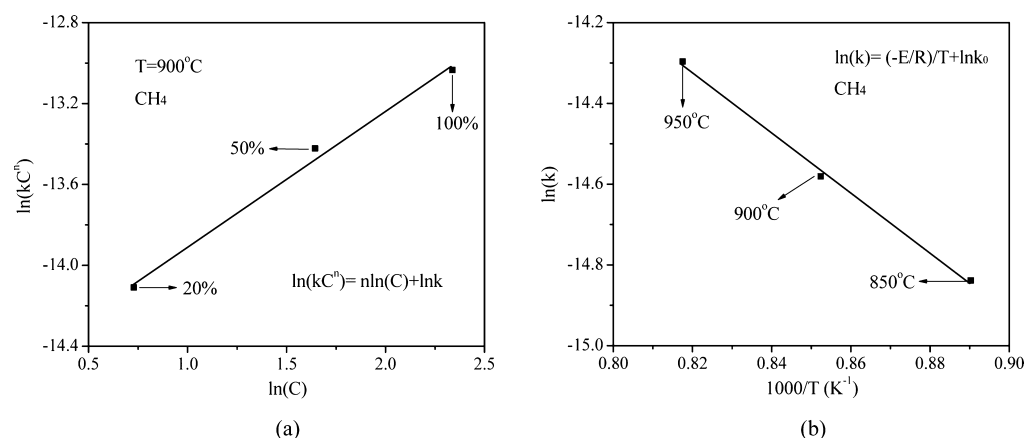$$(-r) = \frac{\rho_m \alpha_s x_{rea}}{b} \frac{dX_{ap}}{dt} \tag{9}$$

**Figure 7.** Procedure to derive the kinetics parameters: (a) plot of $\ln(kC^n) - \ln(C)$; (b) Arrhenius plot of $\ln(k) - 1/T$.

where $r$ is the reaction rate, $\alpha_s$ is the volume fraction of the solid phase, and $x_{rea}$ is the mass fraction of the solid reactants in the OC.

Because the value of $R_{O,ap}$ has been determined, the applicable conversion of OC $X_{ap}$ under every experimental condition can be calculated by eq 5. Then the average value of $kC^n$ can be calculated by eq 7. Thus, as shown in Figure 7a, the fitting lines of $\ln(kC^n) - \ln(C)$ can be further obtained by taking the logarithm of $kC^n$, while $\ln(C)$ can be easily calculated under each fixed temperature. In these fitting lines, the intercept represents $\ln(k)$, and the slope refers to the reaction order $n$. The mean reaction order for $CH_4$ within the range of the investigated temperatures is 0.5. Then, as shown in Figure 7b, the fitting lines of $\ln(k) - 1/T$ can be obtained by taking the logarithm of the Arrhenius equation (i.e., eq 8), from which the apparent activation energy $E$ and the preexponential factor $k_0$ can be further acquired. Eventually, the values of the apparent activation energy $E$ and the preexponential factor $k_0$ for $CH_4$ are found to be 62 kJ/mol and $2.7 \times 10^{-4}$ $mol^{1-n} \cdot m^{3n-2}/s$, respectively. The kinetics parameters for CO can be obtained using the same procedure, and the relevant values are 0.5 for $n$, 56 kJ/mol for $E$, and $1.5 \times 10^{-3}$ $mol^{1-n} \cdot m^{3n-2}/s$ for $k_0$. Table S3 details the kinetics parameters of the calcined lean iron ore with $CH_4$ and CO. It can be seen that the activation energy for CO is lower than that for $CH_4$, indicating CO as the reducing agent is more favorable for reduction of the investigated lean iron ore.[28] This conclusion is consistent with the experimental observation shown above (see section 3.1.4).

## 4. CONCLUSIONS

The CLC with a Chinese sulfur-containing lean iron ore as the OC was conducted in a TGA reactor using two main products of solid-fuel pyrolysis and gasification (i.e., $CH_4$ and CO) as the reducing gases. Long-time reduction/oxidation cycles were carried out to evaluate the cyclic stability and agglomeration tendency of the OC. The effects of the reaction temperature, fuel gas concentration, and fuel gas composition on the reduction reaction were also experimentally investigated. The side reaction of carbon deposition was also discussed. Finally, the SCM with chemical reaction control was adopted to determine the kinetics of the reduction reaction using the experimental data. The following conclusions can be drawn from the present study:

(1) The lean iron ore investigated exhibits good cyclic stability and low tendency for agglomeration in the repeated redox cycles. Moreover, the high contents of $Fe_2O_3$ and inert supports in the lean iron ore as well as the suitable reaction temperatures ($\leq 950$ °C) can restrain the release of $SO_2$ in order to maintain the OC's oxygen-transport capacity.

(2) The reduction rate and reaction degree of the OC can be promoted by increasing the reactor temperature or fuel gas concentration, although the temperature plays a more important role. CO shows much higher reduction reactivity than $CH_4$, which indicates that the iron ore used in this study should be more appropriate for solid-fuel CLC applications.

(3) Carbon deposition was observed for the cases of 50% $CH_4$ and 100% $CH_4$ at the end of the reduction stage when the OC was nearly completely reduced. However, for future solid-fuel CLC systems, only the transformation from $Fe_2O_3$ to $Fe_3O_4$ is desirable in order to get full fuel gas conversion and the concentration of $CH_4$ is very unlikely to reach anywhere near 20%; therefore, the appearance of carbon deposition becomes almost impossible in practice.

(4) The use of the IRoR method enables analysis on the reduction rate to focus on the global reduction rate of the solid reactants in an OC particle instead of the complex local reduction rates from $Fe_2O_3$ to $Fe_3O_4$ and from $CaSO_4$ to CaS. The SCM with chemical reaction control has been adopted to determine the reaction kinetics of OC and acquire relevant kinetics parameters.

Overall, considering the cyclic stability, reactivity, tendency for agglomeration, and cost of the material, the Chinese sulfur-containing lean iron ore investigated in this study can be considered to have a competitive performance against high-grade iron minerals for its use in solid-fuel CLC systems.

## ■ ASSOCIATED CONTENT

### ⓢ Supporting Information

The Supporting Information is available free of charge on the ACS Publications website at DOI: 10.1021/acs.iecr.5b03660.

XRF spectrometry characterization of the calcined iron ore (Table S1), compositions (vol %) and roles of the gases used in the experiments (Table S2), and reaction kinetics parameters of the calcined lean iron ore with $CH_4$ and CO (Table S3) (PDF)

## ■ AUTHOR INFORMATION

**Corresponding Authors**
*Tel.: +44-115-8467674. Fax: +44-115-9513159. E-mail: liu.hao@nottingham.ac.uk.
*Tel.: +86-25-83794744. Fax: +86-25-83795508. E-mail: bsjin@seu.edu.cn.

**Notes**
The authors declare no competing financial interest.

## ■ REFERENCES

(1) Fan, L. S. *Chemical Looping Systems for Fossil Energy Conversions*; Wiley-AIChE: New York, 2010.

(2) Lyngfelt, A.; Leckner, B.; Mattisson, T. A fluidized-bed combustion process with inherent $CO_2$ separation; application of chemical-looping combustion. *Chem. Eng. Sci.* **2001**, *56*, 3101.

(3) Cao, Y.; Pan, W. P. Investigation of chemical looping combustion by solid fuels. 1. Process analysis. *Energy Fuels* **2006**, *20*, 1836.

(4) Berguerand, N.; Lyngfelt, A. Design and operation of a 10 kWth chemical-looping combustor for solid fuels-Testing with South African coal. *Fuel* **2008**, *87*, 2713.

(5) Leion, H.; Mattisson, T.; Lyngfelt, A. Solid fuels in chemical looping combustion. *Int. J. Greenhouse Gas Control* **2008**, *2*, 180.

(6) Shen, L. H.; Wu, J. H.; Xiao, J. Experiments on chemical looping combustion of coal with a NiO based oxygen carrier. *Combust. Flame* **2009**, *156*, 721.

(7) Xiao, R.; Song, Q. L.; Song, M.; Lu, Z. J.; Zhang, S.; Shen, L. H. Pressurized chemical-looping combustion of coal with an iron ore based oxygen carrier. *Combust. Flame* **2010**, *157*, 1140.

(8) Abad, A.; Gayán, P.; de Diego, L. F.; García-Labiano, F.; Adánez, J. Fuel reactor modelling in chemical-looping combustion of coal: 1. Model formulation. *Chem. Eng. Sci.* **2013**, *87*, 277.

(9) García-Labiano, F.; de Diego, L. F.; Gayán, P.; Abad, A.; Adánez, J. Fuel reactor modelling in chemical-looping combustion of coal: 2. Simulation and optimization. *Chem. Eng. Sci.* **2013**, *87*, 173.

(10) Cuadrat, A.; Abad, A.; Gayán, P.; de Diego, L. F.; GarcíaLabiano, F.; Adánez, J. Theoretical approach on the CLC performance with solid fuels: Optimizing the solids inventory. *Fuel* **2012**, *97*, 536.

(11) Wang, X.; Jin, B.; Zhang, Y.; Zhang, Y.; Liu, X. Three Dimensional Modeling of a Coal-Fired Chemical Looping Combustion Process in the Circulating Fluidized Bed Fuel Reactor. *Energy Fuels* **2013**, *27*, 2173.

(12) Wang, X.; Jin, B.; Liu, X.; Zhang, Y.; Liu, H. Experimental investigation on flow behaviors in a novel in situ gasification chemical looping combustion apparatus. *Ind. Eng. Chem. Res.* **2013**, *52*, 14208.

(13) Wang, X.; Jin, B.; Liu, H.; Wang, W.; Liu, X.; Zhang, Y. Optimization of in-situ Gasification Chemical Looping Combustion through Experimental Investigations with a Cold Experimental System. *Ind. Eng. Chem. Res.* **2015**, *54*, 5749.

(14) Adánez, J.; de Diego, L. F.; García-Labiano, F.; Gayán, P.; Abad, A.; Palacios, J.M. Selection of oxygen carriers for chemical-looping combustion. *Energy Fuels* **2004**, *18*, 371.

(15) de Diego, L. F.; García-Labiano, F.; Adánez, J.; Gayán, P.; Abad, A.; Corbella, B. M.; Palacios, J. M. Development of Cu-based oxygen carriers for chemical-looping combustion. *Fuel* **2004**, *83*, 1749.

(16) Abad, A.; Adánez, J.; García-Labiano, F.; de Diego, L. F.; Gayán, P.; Celaya, J. Mapping of the range of operational conditions for Cu-, Fe-, and Ni-based oxygen carriers in chemical-looping combustion. *Chem. Eng. Sci.* **2007**, *62*, 533.

(17) Zafar, Q.; Abad, A.; Mattisson, T.; Gevert, B.; Strand, M. Reduction and oxidation kinetics of $Mn_3O_4/Mg-ZrO_2$ oxygen carrier particles for chemical-looping combustion. *Chem. Eng. Sci.* **2007**, *62*, 6556.

(18) Chuang, S. Y.; Dennis, J. S.; Hayhurst, A. N.; Scott, S. A. Development and performance of Cu-based oxygen carriers for chemical-looping combustion. *Combust. Flame* **2008**, *154*, 109.

(19) Abad, A.; García-Labiano, F.; de Diego, L. F.; Gayán, P.; Adánez, J. Reduction kinetics of Cu-, Ni-, and Fe-Based oxygen carriers using syngas ($CO+H_2$) for chemical-looping combustion. *Energy Fuels* **2007**, *21*, 1843.

(20) Abad, A.; Mattisson, T.; Lyngfelt, A.; Rydén, M. Chemical-looping combustion in a 300W continuously operating reactor system using a manganese-based oxygen carrier. *Fuel* **2006**, *85*, 1174.

(21) Lyngfelt, A.; Thunman, H. Construction and 100 h of operational experience of a 10-kW chemical-looping combustor. *Carbon Dioxide Capture for Storage in Deep Geologic Formations; Results from the CO₂ Capture Project*; Elsevier BV: Amsterdam, The Netherlands, 2005; Vol. *1*, p 625.

(22) de Diego, L. F.; García-Labiano, F.; Gayán, P.; Celaya, J.; Palacios, J. M.; Adánez, J. Operation of a 10 kWth chemical-looping combustor during 200 h with a $CuO-Al_2O_3$ oxygen carrier. *Fuel* **2007**, *86*, 1036.

(23) Adánez, J.; Dueso, C.; de Diego, L. F.; García-Labiano, F.; Gayán, P.; Abad, A. Methane combustion in a 500 Wth chemical-looping combustion system using an impregnated Ni-based oxygen carrier. *Energy Fuels* **2009**, *23*, 130.

(24) Adánez, J.; Cuadrat, A.; Abad, A.; Gayán, P.; de Diego, L. F.; García-Labiano, F. Ilmenite activation during consecutive redox cycles in chemical-looping combustion. *Energy Fuels* **2010**, *24*, 1402.

(25) Berguerand, N.; Lyngfelt, A. The use of petroleum coke as fuel in a 10kWₜₕ chemical-looping combustor. *Int. J. Greenhouse Gas Control* **2008**, *2*, 169.

(26) Berguerand, N.; Lyngfelt, A. Chemical-looping combustion of petroleum coke using ilmenite in a 10 kWₜₕ unit-high-temperature operation. *Energy Fuels* **2009**, *23*, 5257.

(27) Berguerand, N.; Lyngfelt, A. Batch testing of solid fuels with ilmenite in a 10 kWₜₕ chemical-looping combustor. *Fuel* **2010**, *89*, 1749.

(28) Monazam, E. R.; Breault, R. W.; Siriwardane, R. Reduction of hematite ($Fe_2O_3$) to wüstite (FeO) by carbon monoxide (CO) for chemical looping combustion. *Chem. Eng. J.* **2014**, *242*, 204.

(29) Xiao, R.; Chen, L.; Saha, C.; Zhang, S.; Bhattacharya, S. Pressurized chemical-looping combustion of coal using an iron ore as oxygen carrier in a pilot-scale unit. *Int. J. Greenhouse Gas Control* **2012**, *10*, 363.

(30) Zhang, G.; Ostrovski, O. Effect of preoxidation and sintering on properties of ilmenite concentrates. *Int. J. Miner. Process.* **2002**, *64*, 201.

(31) Pröll, T.; Mayer, K.; Bolhàr-Nordenkampf, J.; Kolbitsch, P.; Mattisson, T.; Lyngfelt, A.; Hofbauer, H. Natural minerals as oxygen carriers for chemical looping combustion in a dual circulating fluidized bed system. *Energy Procedia* **2009**, *1*, 27.

(32) Zheng, M.; Shen, L.; Feng, X. In situ gasification chemical looping combustion of a coal using the binary oxygen carrier natural anhydrite ore and natural iron ore. *Energy Convers. Manage.* **2014**, *83*, 270.

(33) Liu, S.; Lee, D.; Liu, M.; Li, L.; Yan, R. Selection and application of binders for $CaSO_4$ oxygen carrier in chemical-looping combustion. *Energy Fuels* **2010**, *24*, 6675.

(34) Tian, H.; Guo, Q. Investigation into the behavior of reductive decomposition of calcium sulfate by carbon monoxide in chemical-looping combustion. *Ind. Eng. Chem. Res.* **2009**, *48*, 5624.

(35) Bidwe, A. R.; Mayer, F.; Hawthorne, C.; Charitos, A.; Schuster, A.; Scheffknecht, G. Use of ilmenite as an oxygen carrier in chemical looping combustion-batch and continuous dual fluidized bed investigation. *Energy Procedia* **2011**, *4*, 433.

(36) Schwebel, G. L.; Leion, H.; Krumm, W. Comparison of natural ilmenites as oxygen carriers in chemical-looping combustion and influence of water gas shift reaction on gas composition. *Chem. Eng. Res. Des.* **2012**, *90*, 1351.

(37) Copeland, R. J.; Alptekin, G.; Cesario, M.; Gebhard, S.; Gershanovich, Y. A novel $CO_2$ separation system. *Proceedings of the First National Conference on Carbon Sequestration*, Washington, DC, 2001.

(38) Kronberger, B.; Loffler, G.; Hofbauer, H. Simulation of mass and energy balances of a chemical-looping combustion system. *Clean Air* **2005**, *6*, 1.

(39) Jerndal, E.; Mattisson, T.; Lyngfelt, A. Thermal analysis of chemical-looping combustion. *Chem. Eng. Res. Des.* **2006**, *84*, 795.

(40) Cho, P.; Mattisson, T.; Lyngfelt, A. Carbon formation on nickel and iron oxide-containing oxygen carriers for chemical-looping combustion. *Ind. Eng. Chem. Res.* **2005**, *44*, 668.

(41) Johansson, M.; Mattisson, T.; Lyngfelt, A. Creating a synergy effect by using mixed oxides of iron-and nickel oxides in the combustion of methane in a chemical-looping combustion reactor. *Energy Fuels* **2006**, *20*, 2399.

(42) Song, Q.; Xiao, R.; Deng, Z.; Zhang, H.; Shen, L.; Xiao, J.; Zhang, M. Chemical-looping combustion of methane with $CaSO_4$ oxygen carrier in a fixed bed reactor. *Energy Convers. Manage.* **2008**, *49*, 3178.

(43) Donskoi, E.; McElwain, D. L. S.; Wibberley, L. J. Estimation and modeling of parameters for direct reduction in iron ore/coal composites: Part II. Kinetic parameters. *Metall. Mater. Trans. B* **2003**, *34*, 255.

(44) Abad, A.; Adánez, J.; Cuadrat, A.; García-Labiano, F.; Gayán, P.; De Diego, L. F. Kinetics of redox reactions of ilmenite for chemical-looping combustion. *Chem. Eng. Sci.* **2011**, *66*, 689.

(45) Garcia-Labiano, F.; Adanez, J.; de Diego, L. F.; Gayán, P.; Abad, A. Effect of pressure on the behavior of copper-, iron-, and nickel-based oxygen carriers for chemical-looping combustion. *Energy Fuels* **2006**, *20*, 26.